Journal of Power Sources 217 (2012) 464–469

Contents lists available at SciVerse ScienceDirect

Journal of Power Sources

journal homepage: www.elsevier.com/locate/jpowsour

Short communication

In situ synchrotron diffraction study of charge–discharge mechanism of sol–gel synthesized $LiM_{0.5}Mn_{1.5}O_4$ (M = Fe, Co)

Aiswarya Bhaskar [a,b,*], Natalia N. Bramnik [a], Dmytro M. Trots [c], Hartmut Fuess [a], Helmut Ehrenberg [a,b,d]

[a] Institute for Materials Science, Technische Universität Darmstadt, Petersenstr. 23, D-64287 Darmstadt, Germany
[b] Institute for Complex Materials, IFW Dresden, Helmholtzstr. 20, D-01069 Dresden, Germany
[c] Bavarian Research Institute of Experimental Geochemistry and Geophysics, University of Bayreuth, Universitätsstr. 30, D-95440 Bayreuth, Germany
[d] Karlsruhe Institute of Technology (KIT), Institute for Applied Materials (IAM), Hermann-von-Helmholtz-Platz 1, D-76344 Eggenstein-Leopoldshafen, Germany

HIGHLIGHTS

- We report the mechanisms of Li-intercalation/-de-intercalation in $LiM_{0.5}Mn_{1.5}O_4$ (M = Fe, Co) spinels.
- The investigation of the mechanism was done by *in situ* synchrotron diffraction.
- The $LiM_{0.5}Mn_{1.5}O_4$ (M = Fe, Co) spinels show a solid-solution mechanism of charge–discharge.

ARTICLE INFO

Article history:
Received 22 February 2012
Received in revised form
21 May 2012
Accepted 5 June 2012
Available online 13 June 2012

Keywords:
Electrochemical mechanism
In situ
Synchrotron diffraction
High-volt cathode

ABSTRACT

Samples with nominal composition $LiM_{0.5}Mn_{1.5}O_4$ (M = Fe, Co) were synthesized via a sol–gel process with a post thermal treatment at 1000 °C. In contrast to the Ni-analogue Co- and Fe-doped samples show a fast degradation at 55 °C with an average capacity retention at RT of ~55% for the Co- and of ~59% for the Fe-substituted samples, respectively after 70 cycles for a C/2 rate. The PITT plots of the Fe doped spinel exhibited a sharp peak in the discharge capacity when cycled with a cut-off current rate C/5, which was assumed due to a kinetic limitation, which disappears when cycled at slower charge–discharge rates. This assumption was checked, and the mechanisms of Li-intercalation/-de-intercalation were investigated in detail for the Fe and Co doped spinels by *in situ* synchrotron diffraction. The charge–discharge processes take place through a solid-solution mechanism in both cases, though the Fe-doped spinel exhibits a two-phase region during the discharge.

1. Introduction

In recent years, transition metal-doped $LiMn_2O_4$ cathodes have received much attention, because of their high operation voltage and increased cycling stability compared to undoped $LiMn_2O_4$. Of these transition-metal substituted spinels, $LiNi_{0.5}Mn_{1.5}O_4$ has been a well- investigated material which exists in two crystallographic structures, one belonging to $Fd\bar{3}m$ space group (cation-disordered) and the other belonging to $P4_332$ space group (cation-ordered). Depending on the initial crystallographic structures, $LiNi_{0.5}Mn_{1.5}O_4$ undergoes different mechanisms of Li extraction–intercalation during cycling [2–5]. While the ordered $LiNi_{0.5}Mn_{1.5}O_4$ undergoes a topotactic phase transitions among three different cubic phases during cycling, the charge–discharge mechanism of the disordered material takes place through a one topotactic phase transition between two different cubic phases when cycled in the voltage range 3.5–5.0 V [5].

Other known substituted spinels include $LiCo_{0.5}Mn_{1.5}O_4$, $LiFe_{0.5}Mn_{1.5}O_4$, $LiCrMnO_4$ etc. Among these materials, $LiCo_{0.5}Mn_{1.5}O_4$ and $LiFe_{0.5}Mn_{1.5}O_4$ are known as 5 V materials since 1998 [6–10]. However, the structural changes during cycling in the 5 V region are not comprehensively investigated. In 2001 Ozhuku et al. have reported a Moessbauer spectroscopy study on the electrochemical reaction mechanism in $LiFe_{0.5}Mn_{1.5}O_4$, which is an interesting candidate for cathode materials due to its environmental and economic advantages [11]. According to them, the lithium-ion insertion into and extraction from the spinel framework of this material take place in a topotactic manner. The redox process taking place around 4.0 V is due to the Mn^{3+}/Mn^{4+} couple and the redox process around 5.0 V is due to the Fe^{3+}/Fe^{4+} couple.

* Corresponding author. Present address: Institute of Physical Chemistry, Westfälische Wilhelms-Universität Münster, Corrensstrasse 28/30, 48149 Muenster, Germany. Tel.: +49 2518336772; fax: +49 2518336032.
E-mail addresses: aiswaryabhaskar@gmail.com, aiswarya.bhaskar@uni-muenster.de (A. Bhaskar).

0378-7753/$ – see front matter © 2012 Elsevier B.V. All rights reserved.
http://dx.doi.org/10.1016/j.jpowsour.2012.06.032

The synthesis, structural and morphological characterization and electrochemical performances of the $LiM_{0.5}Mn_{1.5}O_4$ (M = Ni, Co and Fe) were already described in detail [1], and a comparison was provided between samples with two different thermal treatments. Since the delithiation mechanism of Ni doped spinel has been previously extensively discussed and the mechanism of charge–discharge processes in $LiM_{0.5}Mn_{1.5}O_4$ (M = Co and Fe) with much more pronounced fatigue is not yet well studied, in this work the structural changes of $LiM_{0.5}Mn_{1.5}O_4$ (M = Co and Fe) were elucidated using *in situ* synchrotron diffraction during the first charging–discharging processes in the voltage range of 3.0–5.5 V.

2. Experimental

The samples with final calcination temperature of 1000 °C, which were referred as $LiM_{0.5}Mn_{1.5}O_4$-1000 (M = Co and Fe) in the previous work, were used for the investigation of the underlying electrochemical mechanism [1]. The cathodes for the *in situ* measurements were prepared using a mixture of 80% (w/w) of the active material with 10% (w/w) super P Li carbon (TIMCAL) and 10% (w/w) poly(vinylidenefluoride) 6020 binder, PVdF, (Solvay Solexis) by grinding with *N*-methyl-2-pyrrolidone, NMP, (Fluka). About 50 mg of the mixture was then pressed into a pellet with a pressure of 8 tons and dried at 120 °C for 24 h in vacuum to remove the residual NMP and traces of water. The prepared cathodes were then weighed in the Ar-box before use. Modified Swagelok-type cells, specially designed for *in situ* measurements [12] which consist of an aluminum cathode holder and a stainless steel anode holder as current collectors, were used for the electrochemical measurements and were assembled in an Ar-filled dry box with Li foil as the anode material and a glass-fibre separator soaked with 1M $LiPF_6$ in EC:DMC (1:2) electrolyte. *in situ* synchrotron diffraction was carried out at the powder diffraction beamline B2 [13] of the "Deutsches Elektronensynchrotron" (DESY) at Hamburg, Germany. In order to perform the diffraction measurements, the prepared cells were mounted on a flat sample holder, which was oscillated so as to reduce preferred orientation effects and to achieve a good averaging between different crystallites. Electrochemical tests were performed using a multichannel potentiostatic–galvanostatic system VMP-3 (Biologic, USA). Galvanostatic cycling measurements were carried out between 3.0 V and 5.5 V at a rate C/8. The diffraction measurement was started simultaneously with the electrochemical measurement and continued with a time interval of ~10 min till the end of the first cycle. A wavelength of λ = 0.65168(1) Å was selected by a double-crystal Si (111) monochromator. The diffraction data of the 1st cycle were recorded using the on-site readable image-plate detector OBI [14]. Rietveld refinement was applied for data analysis using the WinplotR package [15]. The standard deviations of all refined parameters were calculated, taking correlations into account [16].

3. Results and discussion

The charge–discharge potential profiles of the first cycles for $LiCo_{0.5}Mn_{1.5}O_4$-1000 and $LiFe_{0.5}Mn_{1.5}O_4$-1000 are displayed in Fig. 1a and b, respectively. The cycling started with Li^+ extraction from $LiM_{0.5}Mn_{1.5}O_4$ (M = Co and Fe) and delivered a capacity of 147 and 137 $mAhg^{-1}$ for Fe and Co substituted samples, respectively. The delivered discharge capacity was lower than that of the charge capacity and was found to be 132 $mAhg^{-1}$ for M = Fe and 110 $mAhg^{-1}$ for M = Co substituted samples. The plots of "remaining number of moles of Li (z)" vs. voltage are shown in the insets of each figure. About ~0.9 and ~0.8 mol of Li are intercalated back in the case of $LiFe_{0.5}Mn_{1.5}O_4$-1000 and $LiCo_{0.5}Mn_{1.5}O_4$-1000 at the end of the first cycles. Two plateaus are visible in the

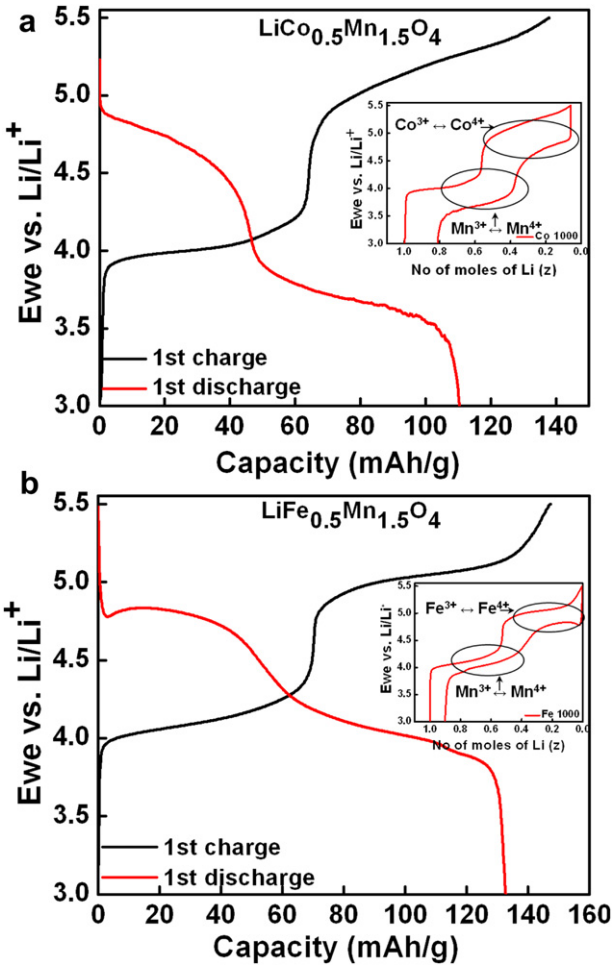

Fig. 1. The first charge–discharge potential profiles of a) $LiCo_{0.5}Mn_{1.5}O_4$-1000, b) $LiFe_{0.5}Mn_{1.5}O_4$-1000. Inset: plots of voltage vs. number of moles of remaining Li (z), for the corresponding samples.

case of both samples in ranges of ~3.9–4.3 and 4.9–5.3 which corresponds to the electrochemical reactions of the Mn^{3+}/Mn^{4+} couple and M^{3+}/M^{4+}, respectively. The results of galvanostatic cycling at C/8 are displayed in Fig. 2 and show capacity retentions of

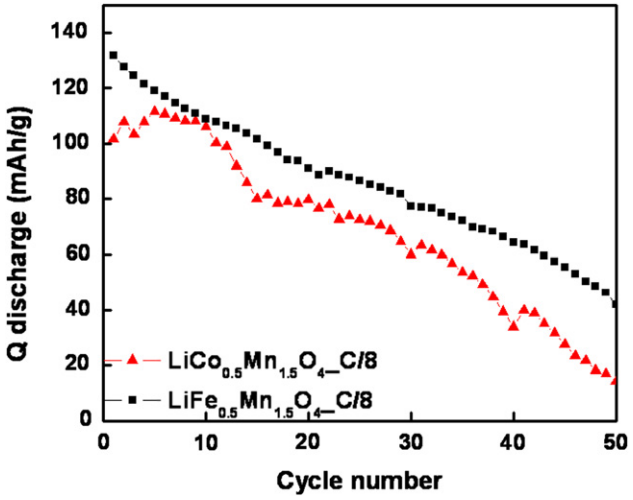

Fig. 2. Cycle number vs. discharge capacity plots for $LiCo_{0.5}Mn_{1.5}O_4$-1000 and $LiFe_{0.5}Mn_{1.5}O_4$-1000, with a charge–discharge rate C/8 at RT in the voltage range 3.0–5.5 V.

32% for Fe doped and 14% for Co doped samples, which are much lower in comparison with the capacity retentions for the same samples cycled at a rate of C/2 in the voltage range 3.5–5.3 (~55% for Co and ~59% for Fe after 70 cycles [1]). This stronger fatigue is expected for the broader voltage range and slower cycling, which promotes parasitic reactions.

Fig. 3a and b shows the *in situ* diffraction patterns of the cells freshly prepared, after the end of first charge and at the end of the first cycle for $LiCo_{0.5}Mn_{1.5}O_4$-1000 and $LiFe_{0.5}Mn_{1.5}O_4$-1000, respectively. The Rietveld refinement was based on the structural models as described in a previous work [1]. The upper line of reflections belongs to the spinel phase in $Fd\bar{3}m$ space group, the lower line to the Al current collector window. A profile matching mode was used for the Al reflections instead of a Rietveld refinement, because their intensities are dominantly affected by texturing and, therefore, deviate from those of an ideal Al powder. Rietveld refinements confirm that the spinel structure with $Fd\bar{3}m$ space group is appropriate to describe the crystal structure at the end of charge and after the complete cycle. The lattice parameters of delithiated $Fd\bar{3}m$ spinels are expectantly lower comparing to the initial phases (see Table 1). The calculated shrinkages of the unit cell due to lithium extraction at the end of the first charge are 1.55% and 2.35% for $LiCo_{0.5}Mn_{1.5}O_4$-1000 and $LiFe_{0.5}Mn_{1.5}O_4$-1000, respectively. After the first cycle the unit cell parameters became closer to the initial values again and were even slightly higher. Two effects are contributing to the increase of the lattice parameter:

1. The successful re-intercalation of Li^+ back into the spinel structure. However, this effect can only explain the reincrease up to the initial value.

Table 1
Refinement results based on *in situ* synchrotron diffraction, for $LiM_{0.5}Mn_{1.5}O_4$-1000 (M = Fe, Co), space group $Fd\bar{3}m$, at different stages of cycling.

Sample	Freshly prepared cell	End of 1st charge	End of 1st cycle
	a (Å)	a (Å)	a (Å)
$LiFe_{0.5}Mn_{1.5}O_4$-1000	8.2520(4)	8.0581(4)	8.2533(6)
$LiCo_{0.5}Mn_{1.5}O_4$-1000	8.1420(3)	8.0158(2)	8.1440(3)

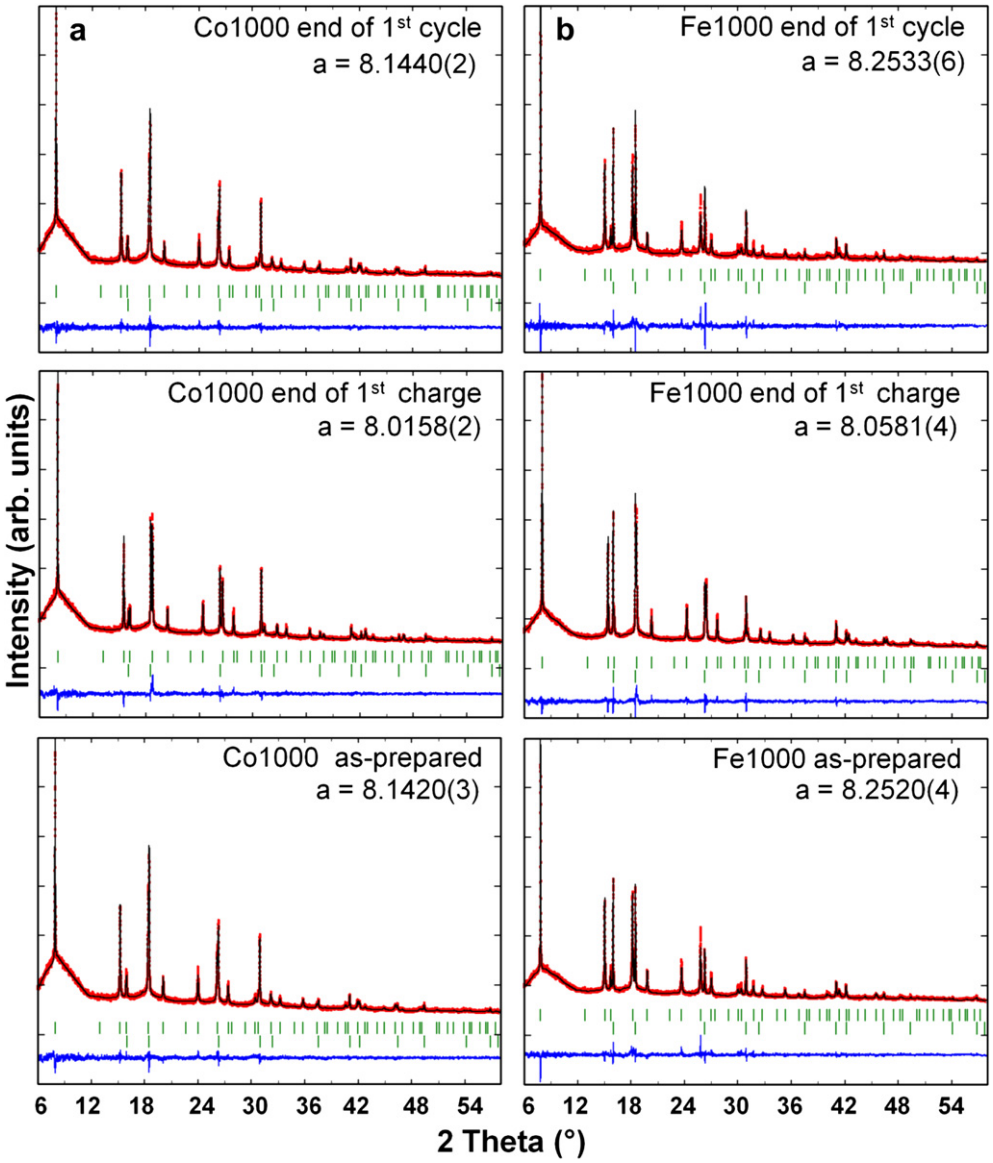

Fig. 3. Rietveld refinement results based on *in situ* synchrotron diffraction data for (a) $LiCo_{0.5}Mn_{1.5}O_4$-1000 (b) $LiFe_{0.5}Mn_{1.5}O_4$-1000 in space group $Fd\bar{3}m$ for as prepared cells, at the end of 1st charge and at the end of 1st cycle.

2. A loss of oxygen introduces a partial reduction of Mn^{4+} to Mn^{3+} and hereby an expansion of the lattice parameter.

The observed slightly larger value for the lattice parameter after the first cycle is therefore an indication for a high degree of reversible Li-insertion and a hint to some irreversible oxygen loss during the highly charged state. These two effects, however, cannot be quantitatively distinguished.

The structure evolutions during charge and discharge processes for both Co and Fe substituted samples are displayed in Fig. 4a and b with selected 2θ regions, respectively $19.8° \leq 2\theta \leq 24.8°$ for Co- and $19.6° \leq 2\theta \leq 24.5°$ for Fe − doped samples, where red and blue pattern lines correspond to charge and discharge regions, respectively. The diffraction patterns from $LiCo_{0.5}Mn_{1.5}O_4$-1000 display shifting reflection peaks during charge and discharge without appearance of any additional reflections. Therefore, the delithiation and lithium reinsertion into $LiCo_{0.5}Mn_{1.5}O_4$ occurs as a solid-solution reaction in the applied voltage range. The evolution of lattice parameters is shown in Fig. 5a. In the case of $LiFe_{0.5}Mn_{1.5}O_4$-1000 the delithiation occurs mainly via solid-solution mechanism as well. However, during the first lithium reinsertion, a second spinel phase appears in the range $0.09 \leq Z \leq 0.53$, with the same space group $Fd\bar{3}m$, but with slightly different lattice parameters. This region is represented by green lines in Fig. 4b. One of the diffraction patterns which show the co-existence of two phases during discharge is shown in Fig. 6 and the regions, where the two phases are clearly visible, are zoomed in. The PITT experiments performed on $LiFe_{0.5}Mn_{1.5}O_4$-1000 showed that this material exhibit a sharp peak at the discharge capacity region around 5 V in the first cycle [1]. Such a sharp PITT peak, characteristic of two-phase mechanism, agrees very well with two-phase behaviour

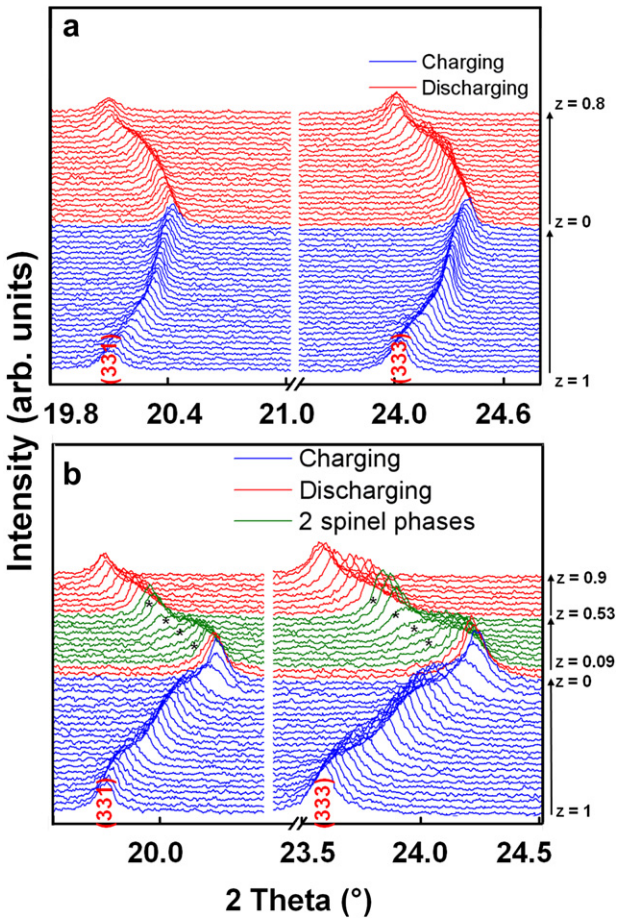

Fig. 4. The selected 2θ regions of the total 47 and 43 *in situ* synchrotron diffraction patterns of $LiCo_{0.5}Mn_{1.5}O_4$-1000 (a) and $LiFe_{0.5}Mn_{1.5}O_4$-1000 (b) respectively, during the 1st cycle. The diffraction peaks marked by "*" in (b) are assigned to the second spinel phase.

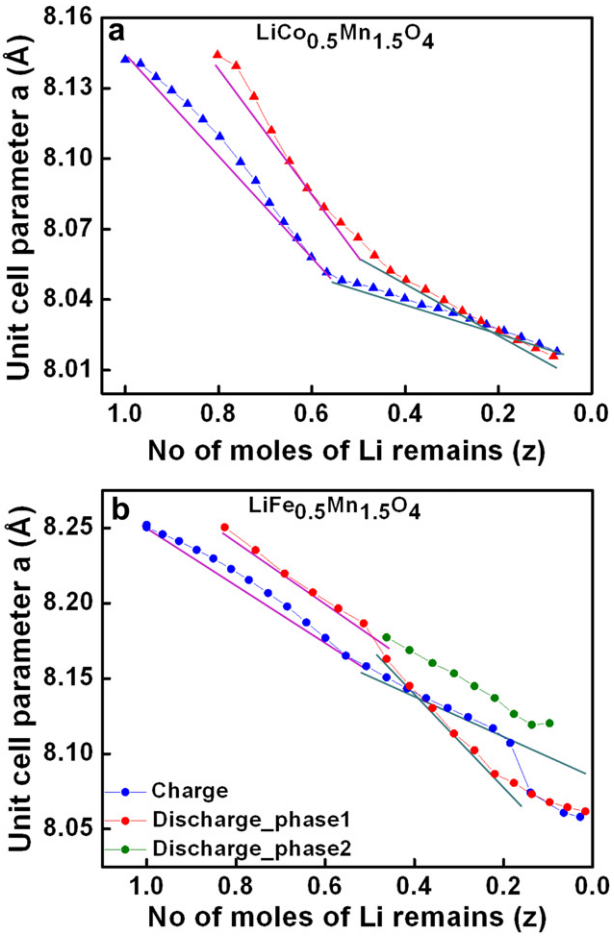

Fig. 5. Change in the unit cell parameter as a function of z in (a) $Li_zCo_{0.5}Mn_{1.5}O_4$-1000 and (b) $Li_zFe_{0.5}Mn_{1.5}O_4$-1000. The half-filled circles in (b) represent the unit cell parameter changes of the additional spinel phase observed during discharging in the Fe-doped sample.

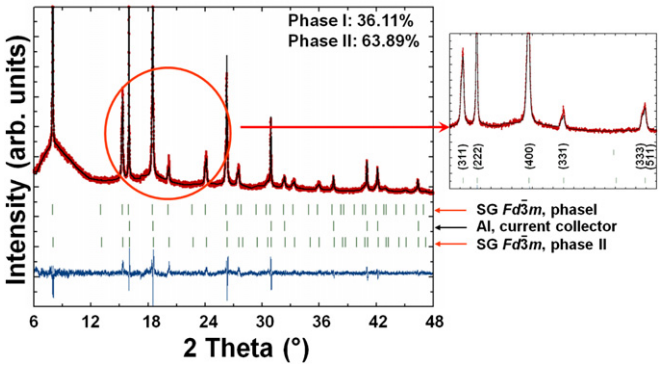

Fig. 6. *In situ* synchrotron diffraction pattern corresponds to 0.25 moles of Li re-intercalation in $LiFe_{0.5}Mn_{1.5}O_4$-1000 where a pronounced co-existence of the two spinel phases is observed. The lattice parameters and the corresponding phase ratio were found as 8.145(2), 8.101(1) and 36.60 (0.75) %, 63.40 (1.02) % for phase I and phase II respectively.

revealed by synchrotron diffraction of $LiFe_{0.5}Mn_{1.5}O_4$-1000. Nevertheless, sharp discharge peak was shown to transform into broad one when cycled at a slower rate. Therefore, one can suppose, that the two-phase behaviour may result from poor kinetic of lithium-reinsertion process in the first cycle. It should be noted, that such a two-phase behaviour upon lithium re-extraction has not been reported for $LiFe_{0.5}Mn_{1.5}O_4$ before. The appearance of this second phase during the first discharge is considered as a formation step, which depends on the specific conditions like charge rate and temperature and results in a better kinetics for Li-reinsertion in the following cycles.

The evolution of the lattice parameter with the extracted Li content for both Co- and Fe-doped spinels is shown in Fig. 5. There are two regions for both the Co- and Fe-doped samples, represented by the two different slopes of the curves (shown by lines in Fig. 5), which may indicate a different charge compensation mechanism. The two slopes may correspond to the Li^+ intercalation and extraction corresponding to the Mn^{3+}/Mn^{4+} and M^{3+}/M^{4+} (M = Co, Fe) electrochemical reactions. The lattice parameters from the second spinel phase of $LiFe_{0.5}Mn_{1.5}O_4$-1000 in the discharge capacity region also increase linearly, which illustrates that this part of the material remains active during the Li re-intercalation, further confirmed by the evolution of phase ratios in the two-phase region (Fig. 7).

The changes in the half width parameters X (Lorentzian broadening), W and the oxygen coordinate "u" during cycling of $LiCo_{0.5}Mn_{1.5}O_4$-1000 are plotted against the amount of remaining Li (z) in the material in Fig. 8a–c. The metal–metal and metal-oxide bond distances are related to the unit cell and the u parameter of the oxygen ions. Any changes in the u parameter also reflect the adjustment of the structure to accommodate differences in the relative cation radii in the octahedral and tetrahedral sites [17]. The X parameter describes a $\tan\theta$ dependence of the half width with Lorentzian profile shape and results mainly from residual strain $\varepsilon = \Delta d/d$. The plot of X parameter vs. number of moles of Li shows that in the region of Mn^{3+}/Mn^{4+} (up to ~0.5 moles of Li extraction) electrochemical reaction, the peaks are much broader and become narrower when more Li is extracted and remains narrow throughout the Co^{3+}/Co^{4+} reaction region. This broadening, which also depends on the distribution of lattice planes could be attributed to microstructure effects of the sample (like stress, strain, crystallite size or disorder) or inhomogeneity in the structure (existence of more spinel structures with lattice parameters of very

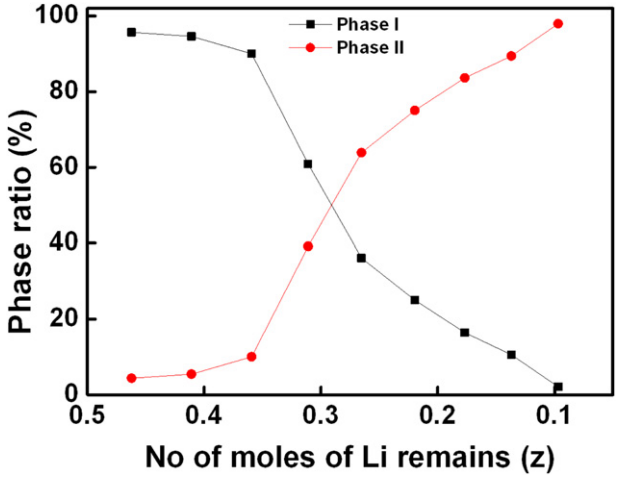

Fig. 7. Phase ratio of the two phases vs. remaining number of moles of lithium during first discharge for $LiFe_{0.5}Mn_{1.5}O_4$-1000 in the region of lithium content (z), $0.09 \le z \le 0.53$.

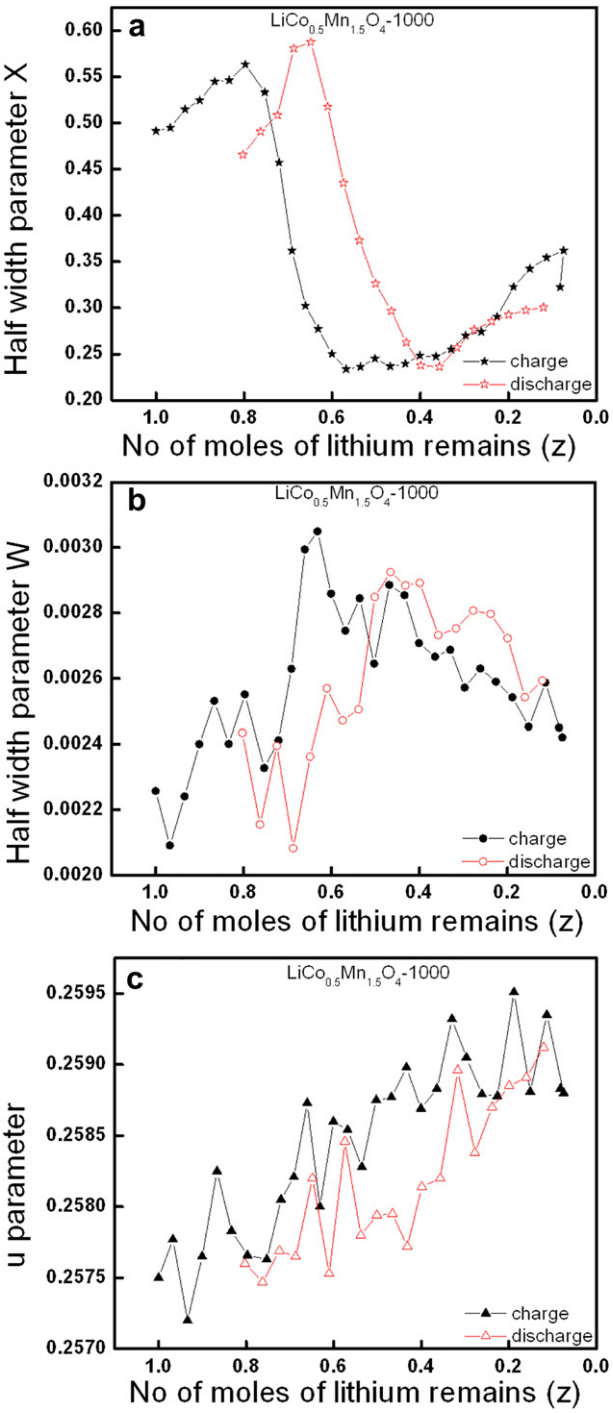

Fig. 8. Change in the half width parameters X, W and the oxygen coordinate u as a function of z in $Li_zCo_{0.5}Mn_{1.5}O_4$-1000.

small difference) or a combined effect. The best possible suggestion is: after the extraction of a half mole of Li, the structure undergoes a conditioning process and the rest of the Li extraction would take place in a more homogeneous manner (narrow peaks). Similarly in the case of Li re-intercalation, after a half mole, the structure should experience a stress which has to be overcome, due to less availability of Li sites, and it again lead to an inhomogeneous Li re-intercalation (broader peaks). Hence a combined effect of stress and inhomogeneity could well explain this anomalous behaviour. Note that several explanations are possible for the observed

broadening of reflections. Most probably, the slow kinetics of Li- and charge-transfer reactions results, in an inhomogeneous distribution of Li over the grains, so that domains with different Li-contents and, therefore, slightly different lattice parameters occur. Such a distribution of lattice parameters is observed also as a broadening of reflections. The regions within one cycle, which suffer from slow kinetics of Li extraction and insertion as revealed from the electrochemical characterization, agree with those showing such a broad distribution of lattice parameters and a high amount of Li in the crystal structure, i.e. a low number of available vacancies on the Li site. Also it can be seen that the values of X parameter during charge and discharge for the same number of moles of Li is different. This could be explained as the Li contents are calculated based on the number of electrons flown and the corresponding diffraction parameters by correlating to the obtained patterns based on the time interval, taking into account that the electrochemical reaction and diffraction experiment begins when the number of moles of Li is "1".

As different from the obvious changes of X parameters during Li extraction and re-intercalation, it is hard to observe the existence of such changes for the *W* and *u* parameters. Therefore, the dominant microstructure effect is of strain type. Note that the very similar evolution of X during charge and discharge with the same absolute values and the same characteristic minima and maxima (only slightly shifted against each other) indicate that the stress states, induced by Li extraction and insertion, seem to be characteristic for the intermediate Li-contents. An effect of changes in the crystallite sizes is rather improbable, because in this case the profile broadening should mainly affect the W parameter, describing a Gaussian shape. Furthermore, the smaller values for the half widths would require a significant and reversible crystallite growth, which is rather implausible.

4. Conclusions

In situ synchrotron diffraction has revealed single solid-solution mechanism for $LiFe_{0.5}Mn_{1.5}O_4$-1000 and $LiCo_{0.5}Mn_{1.5}O_4$-1000. A two-phase region was revealed upon discharge of $LiFe_{0.5}Mn_{1.5}O_4$ in the range of lithium content $0.09 \leq Z \leq 0.53$. The appearance of two-phase region seems to result from slow kinetic of lithium reinsertion. The observed hindered Li-exchange correlates with a broadening of reflections in the corresponding regions of the charge–discharge cycle.

Acknowledgement

Financial support by the "Deutsche Forschungsgemeinschaft" (DFG, EH183/8) is gratefully acknowledged. This work has benefited from beam time allocation by HASYLAB at beamline B2.

References

[1] A. Bhaskar, N.N. Bramnik, A. Senyshyn, H. Fuess, H. Ehrenberg, J. Electrochem. Soc. 157 (2010) A689–A695.
[2] K. Ariyoshi, Y. Iwakoshi, N. Nakayama, T. Ohzuku, J. Electrochem. Soc. 151 (2004) A296–A303.
[3] J.-H. Kim, C.S. Yoon, S.-T. Myung, J. Prakash, Y.-K. Sun, Electrochem. Solid-State Lett. 7 (2004) A216–A220.
[4] S.H. Park, S.-W. Oh, S.H. Kang, I. Belharouak, K. Amine, Y.-K. Sun, Electrochim. Acta 52 (2007) 7226–7230.
[5] J.-H. Kim, S.-T. Myung, C.S. Yoon, S.G. Kang, Y.-K. Sun, Chem. Mater. 16 (2004) 906–914.
[6] H. Kawai, M. Nagata, H. Tukamoto, A.R. West, J. Mater. Chem. 8 (1998) 837–839.
[7] H. Kawai, M. Nagata, M. Tabuchi, H. Tukamoto, A.R. West, Chem. Mater. 10 (1998) 3266–3268.
[8] T. Ohzuku, S. Takeda, M. Iwanaga, J. Power Sources 81–82 (1999) 90–94.
[9] M.Y. Song, D.S. Ahn, S.G. Kang, S.H. Chang, Solid State Ionics 111 (1998) 237–242.
[10] A. Eftekhari, J. Power Sources 124 (2003) 182–190.
[11] T. Ohzuku, K. Ariyoshi, S. Takeda, Y. Sakai, Electrochim. Acta 46 (2001) 2327–2336.
[12] K. Nikolowski, C. Baehtz, N.N. Bramnik, H. Ehrenberg, J. Appl. Crystallogr. 38 (2005) 851–853.
[13] M. Knapp, C. Baehtz, H. Ehrenberg, H. Fuess, J. Synchrotron Rad. 11 (2004) 328–334.
[14] M. Knapp, V. Joco, C. Baehtz, H.H. Brecht, A. Berghaeuser, H. Ehrenberg, H. von Seggern, H. Fuess, Nucl. Instrum. Methods A 521 (2004) 565–570.
[15] T. Roisnel, J. Rodriguez-Carvajal, Mater. Sci. Forum 118 (2001) 378.
[16] J.F. Berar, P. Lelann, J. Appl. Crystallogr. 24 (1991) 1–5.
[17] P. García Casado, I. Rasines, J. Solid State Chem. 52 (1984) 187–193.